ARMY RESEARCH LABORATORY

Characterization of the Effect of Fiber Undulation on Strength and Stiffness of Composite Laminates

by Todd C Henry, Jaret C Riddick, Ryan P Emerson, and Charles E Bakis

ARL-TR-7249 **March 2015**

NOTICES

Disclaimers

The findings in this report are not to be construed as an official Department of the Army position unless so designated by other authorized documents.

Citation of manufacturer's or trade names does not constitute an official endorsement or approval of the use thereof.

Destroy this report when it is no longer needed. Do not return it to the originator.

Army Research Laboratory
Aberdeen Proving Ground, MD 21005-5069

ARL-TR-7249 **March 2015**

Characterization of the Effect of Fiber Undulation on Strength and Stiffness of Composite Laminates

Todd C Henry and Jaret C Riddick
Vehicle Technology Directorate, ARL

Ryan P Emerson
Weapons and Materials Research Directorate, ARL

Charles E Bakis
Pennsylvania State University

REPORT DOCUMENTATION PAGE	Form Approved OMB No. 0704-0188

1. REPORT DATE *(DD-MM-YYYY)*	2. REPORT TYPE	3. DATES COVERED
March 2015	Final	15 May–20 August 2013

4. TITLE AND SUBTITLE
Characterization of the Effect of Fiber Undulation on Strength and Stiffness of Composite Laminates

5a. CONTRACT NUMBER

5b. GRANT NUMBER

5c. PROGRAM ELEMENT NUMBER

6. AUTHOR(S)
Todd C Henry, Jaret C Riddick, Ryan P Emerson, and Charles E Bakis

5d. PROJECT NUMBER

5e. TASK NUMBER

5f. WORK UNIT NUMBER

7. PERFORMING ORGANIZATION NAME(S) AND ADDRESS(ES)
US Army Research Laboratory
ATTN: RDRL-VTM
Aberdeen Proving Ground, MD 21005-5069

8. PERFORMING ORGANIZATION REPORT NUMBER
ARL-TR-7249

9. SPONSORING/MONITORING AGENCY NAME(S) AND ADDRESS(ES)

10. SPONSOR/MONITOR'S ACRONYM(S)

11. SPONSOR/MONITOR'S REPORT NUMBER(S)

12. DISTRIBUTION/AVAILABILITY STATEMENT
Approved for public release; distribution is unlimited.

13. SUPPLEMENTARY NOTES

14. ABSTRACT

Stiffness and strength predictions of undulated composites (filament-wound cylinders, braids, plain weaves, etc.) using traditional laminated composite theories are complicated by complex fiber architecture. Undulations consisting of fibers passing over and under each other result from the interweaving process. In the current investigation, full-field strain measurements were used to evaluate local strain distributions in the region of a 0° undulated ply in a $[0_n/90_n]_s$ laminate (n = 2,4,6) and a 30° undulated ply in a $[30_n/–60_n]_s$ laminate (n = 2,4). Specimens were manufactured with carbon fibers, various amplitudes of undulation, and matrix materials with moduli ranging from 300 to 3,000 MPa. Two-dimensional digital image correlation was used on the free edges of the compressively loaded specimens. The observed strain fields were highly influenced by the undulation geometry. The axial modulus (E_x) of a $[0_n/90_n]_s$ laminate was more sensitive to reinforcement undulation for flexible matrixes (300 MPa) rather than rigid (3,000 MPa). Fiber undulation was observed to elevate out-of-plane shear and through-thickness normal strains in regions eventually involved in the fiber microbuckling failure process.

15. SUBJECT TERMS
composite, laminate, fiber undulation, driveshaft, FMC, microbuckling

16. SECURITY CLASSIFICATION OF:			17. LIMITATION OF ABSTRACT	18. NUMBER OF PAGES	19a. NAME OF RESPONSIBLE PERSON
a. REPORT	b. ABSTRACT	c. THIS PAGE			Todd C Henry
Unclassified	Unclassified	Unclassified	UU	28	19b. TELEPHONE NUMBER (*Include area code*) 410-278-9831

Contents

List of Figures

List of Tables

Acknowledgments

David Gray, Bob Kaste, and Paul Moy are thanked for time dedicated to experimental setup and digital image correlation. The US Army Research Laboratory's Vehicle Technology Directorate is thanked for financial support through the Science, Mathematics and Research for Transformation Fellowship.

INTENTIONALLY LEFT BLANK.

1. Introduction

Fiber-reinforced composites have exceptional tailorability, stiffness, and strength. Flexible matrix composites (FMCs), in particular, are an interesting class of composite composed of very stiff and strong carbon fibers with a relatively compliant elastomeric matrix such as polyurethane. FMCs have been investigated for potential application to helicopter tail rotor driveshafts, where power can be transmitted (stiff in torsion) under misaligned conditions (soft in bending) without complex, maintenance-intensive flexible couplers.[1–5] A single-piece FMC filament-wound driveshaft can potentially replace typical multi-segmented shafts, reducing weight, complexity, and maintenance requirements (Fig. 1). The compliance of the FMC matrix reduces the tendency of the driveshaft to overheat during rapid cyclic loading that would occur during misaligned operation.

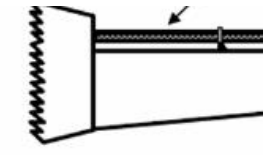

Fig. 1 Traditional driveline (top) and proposed driveline (bottom)[1]

Driveshafts and other composite cylinders are commonly fabricated by wet filament winding wherein tows of fiber are wrapped onto a cylindrical mandrel helically at $\pm\theta$ angles relative to the axial axis. In a single helically wound layer, $-\theta$ tows pass under and over $+\theta$ tows and vice versa, resulting in triangular regions of $\pm\theta$ and $\mp\theta$ laminated material. The triangular regions repeat around the circumference of the cylinder by an integer number known as the filament winding pattern (Fig. 2). At the helical and circumferential borders of these triangles, fibers undulate as they switch from the top layer to the bottom layer and vice versa (Fig. 2).

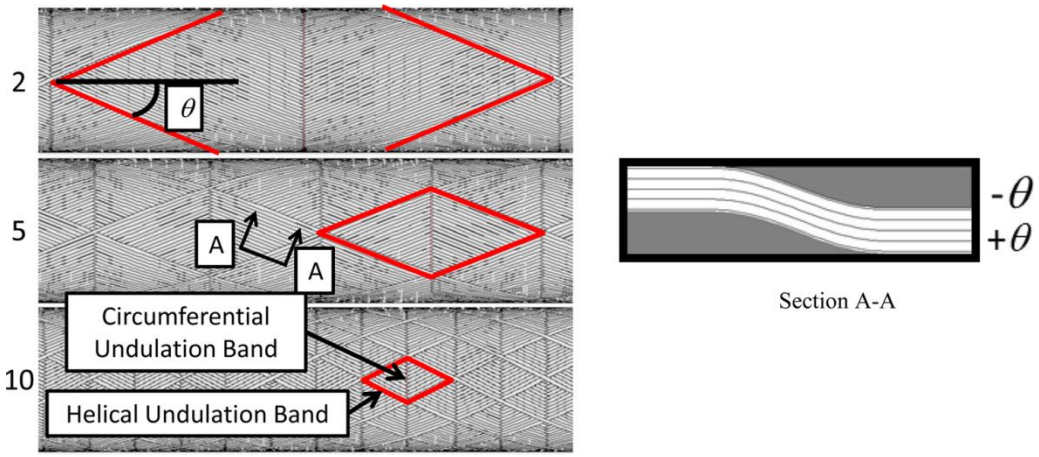

Fig. 2 Filament wound tubes: winding patterns of 2, 5, and 10, showing repeating rhombic units (left) and cross section of undulated helical tow (right)

The out-of-plane orientation of the fiber reduces stiffness and strength.[6] Accurately measuring the geometric size and shape of the undulation is absolutely necessary to estimate reductions in modulus. Ishikawa and Chou[7] introduced several textile composite models, such as the fiber crimp model, to address the effect of fiber undulation for plain and harness satin weaves. The fiber crimp model assumes that classical lamination theory is valid at discrete points along the undulation, employing the hypothesis that the stiffness of the undulated region can be determined by numerical integration with accurate information about the undulation geometry. Ishikawa and Chou[7] reported that the fiber crimp model was fairly accurate in estimating the modulus reducing quality of the fiber undulation. Other reports[8–13] expanded upon Ishikawa and Chou[7] by including nonorthogonally crossing fibers. Three-dimensional fiber orientation was considered although the analysis was truncated to 2 dimensions upon laminate homogenization. The undulated fiber architecture creates complex elastic coupling[9–12] and stress distributions[8,13] at the ply level that have been shown to analytically and experimentally reduce composite axial stiffness (E_x).[6,10–13]

Analytical models for compressive strength of composites generally rely on assumed mechanisms of failure such as for microbuckling or fiber kinking. Microbuckling is the local buckling of fibers embedded within a polymer matrix foundation (Fig. 3a). Kinking is the process by which bands of material experience plastic deformation in regions where the fiber reinforcement has broken (Fig. 3b). Rosen[14] assumed that the fiber reinforcement would buckle either out of phase (extensional mode) or in phase (shear mode). Experimentally measured strength was often below the strength predicted due to imperfect fiber spacing and orientation as well as various flaws and voids. Improvements to Rosen's[14] models stemmed from understanding that the fiber misalignment,[15,16] fiber waviness,[17] and fiber-matrix interfacial strength[18] are all factors in compressive strength prediction. Micromechanical models[13] show

that out-of-plane undulation creates significant shear and normal stress in the plane of the undulation and suggest that accurate knowledge of the undulation geometry is critical to accurate strength prediction.

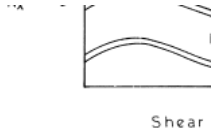

a) Microbuckling failure modes b) Kinking failure mode

Fig. 3 Compression failure modes[19]

Recently developed experimental methods allow for the improved characterization of not only complex strain fields but also failure mechanisms in composite specimens with undulated reinforcement. For example, the digital image correlation (DIC) method, made practical by the advent of measurement-grade digital cameras and high-speed computers, has been used to measure full-field strains in filament-wound cylinders under internal pressure,[20] combined tension, torsion, and bending loads,[21] uniaxial compression,[22] and in compression before and after ballistic impact damage.[23] DIC has also been used to evaluate flat coupons manufactured with ply waviness.[24,25]

The objective of the current investigation was to observe the effects of out-of-plane undulation on the full-field strains and structural behavior of composites under axial compression. Flat composite specimens with carefully manufactured sinusoidal undulations were chosen as a simplified case of fiber undulation in a filament-wound cylinder. A series of $[0_n/90_n]_s$ and $[30_n/–60_n]_s$ laminates with different out-of-plane undulation amplitudes, undulation lengths, and matrix materials were manufactured and tested for this purpose. Two-dimensional DIC was used to measure in-plane surface displacements and strains on the various surfaces of the specimens. Based on these measurements, the onset of failure could be observed in many cases.

2. Experiment/Calculations

Composite specimens were manufactured using AS4D standard modulus carbon fibers (Hexcel Corp., Stamford, CT). Three matrix materials were used in this investigation. The most compliant is a flexible polyurethane prepolymer commonly known as Adiprene LF750, a toluene diisocyanate terminated polyether (Chemtura Corp., Middlebury, CT). An intermediate-modulus flexible polyurethane prepolymer, a toluene diisocyanate polytetramethylene polycaprolactone polyether known as Conathane DPRN 30917 (Cytec Industries, Olean, NY), was selected. For long pot life, a delayed-action diamine curative, Duracure C3LF (Chemtura Corp., Middlebury, CT), was used to cure the polyurethane prepolymers. The highest stiffness matrix for making rigid matrix composites (RMCs) consisted of a bisphenol F epoxide, EPON 862, and an aromatic amine curing agent, Curative W (both from Momentive Specialty Chemicals, Columbus, OH). The tensile modulus of elasticity of the neat matrix materials in the 1,000- to 2,000-με range was measured previously[26]: LF750, 250 MPa; 30917, 980 MPa; and EPON 862, 3,000 MPa. The curing schedule for the polyurethane matrix was 140 °C for 2 h followed by 100 °C for 16 h. The 16-h post-cure for the flexible matrix ensures that there are no aging effects in the variable time period between manufacture and test. The curing schedule for the epoxy matrix is 121 °C for 1 h followed by 177 °C for 2 h.

Impregnated sheets of unidirectionally reinforced composite were manufactured by passing carbon fiber tow through a resin bath and winding the tow onto a flat paddle mandrel with a target fiber volume fraction (V_f) of 50% (Fig. 4). The thickness of the sheets was varied by winding a variable number of unidirectionally oriented layers on to the mandrel, n, where n = 2, 4, or 6. The paddle mandrel was covered by nonporous polytetrafluoroethylene-coated glass fabric from Airtech (Huntington Beach, CA). To create each laminate, 4 sheets of n layers were used. For example, four 2-layer sheets comprise the $[0_2/90_2]_s$ laminate and four 4-layer sheets comprise the $[0_4/90_4]_s$ laminate, etc. All other manufacturing conditions were kept approximately constant for the various thicknesses.

Fig. 4 25.4- × 25.4-cm paddle mandrel[26]

Manufacturing specimens with controlled undulation involves special positioning of the 0° and 90° plies. The unidirectional sheets serving as the 90° plies were first cut in half, then a half-sheet of 90° composite was laid in a mold (Fig. 5a). A whole 0° sheet was then laid over the first half-layer of 90° composite (Fig. 5b), and another half-sheet of 90° composite was added to complete half of the laminate thickness. These steps were repeated in reverse order to create a symmetric laminate with a nearly sinusoidal undulation in the continuous 0° layers (Fig. 5c). The laminate was consolidated in a computer-controlled press at 241 kPa of pressure and the appropriate temperature-time schedule for each matrix material.

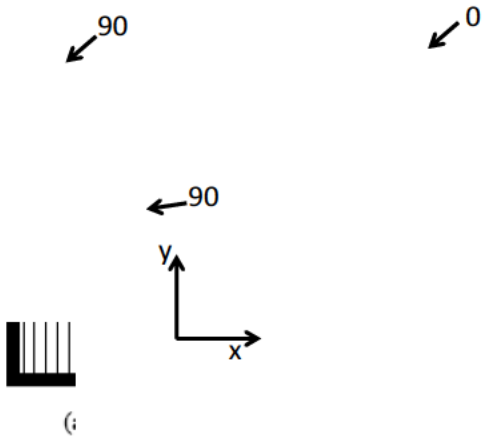

Fig. 5 Undulated specimen layup sequence

After the laminate was removed from the mold, specimens were cut to a length of 140–155 mm and a width of 25.4 mm (Fig. 6). Specimens without undulations are referred to as "nonundulated" specimens. The undulation was placed near the mid-length position of the specimen.

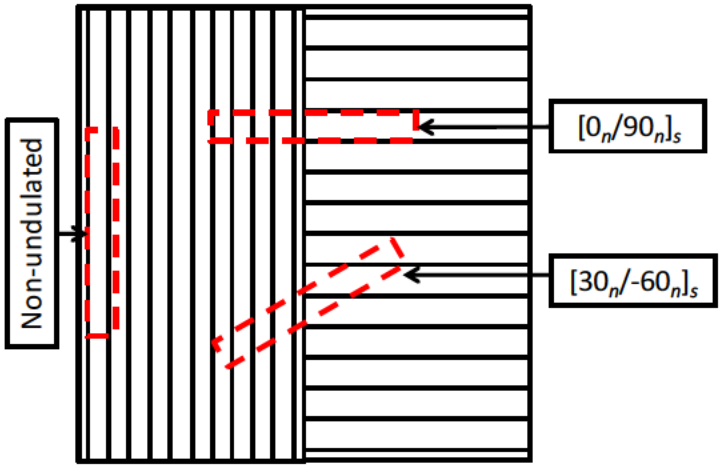

Fig. 6 Specimen orientations in manufactured plates

Specimen inspection before testing revealed that for approximately identical manufacturing conditions, specimens with a higher viscosity matrix at room temperature had a shorter undulation wavelength. The lowest viscosity matrix, EPON 862 (Fig. 7a), followed by LF750 (Fig. 7b), and finally the highest viscosity matrix, 30917 (Fig. 7c), highlight this effect. The manufactured undulation appeared to have an approximately sinusoidal shape across all matrix materials and thicknesses.

(a) EPON 862 (b) LF750 (c) 30917

Fig. 7 Specimen undulation profiles

The geometric parameters of the undulation were taken from photographs of each material system and wave amplitude (Fig. 7) and are tabulated in the following Table. The parameters are presumably identical in the $[0_n/90_n]_s$ and $[30_n/–60_n]_s$ specimens since they were all cut from the same laminate. Distances are measured in pixels using an image analysis tool and converted to millimeters. The amplitudes under investigation vary from approximately 0.6 to 1.8 mm, which translates to approximately 5°–20° of out-of-plane orientation of the fibers. The amplitude of the sine wave is approximately equal to 25% of the laminate thickness because all plies are of roughly equal thickness.

Table Specimen geometric parameters

Material	Number of plies, *n*	Pixels (mm)	Undulation amplitude, *A* (pixels)	Undulation length, *L* (pixels)	Undulation amplitude, *A* (mm)	Undulation length, *L* (mm)	*A*/*L*	Ply thickness (mm)	Estimated fiber volume content, V_f (%)
LF750	2	46	34	291	0.73	6.33	0.10	0.36	48
	4	46	61	319	1.32	6.93	0.17	0.33	
	6	46	87	395	1.89	8.59	0.23	0.32	
DPRN 30917	2	48	32	236	0.67	4.92	0.12	0.33	47
	4	48	66	261	1.36	5.44	0.19	0.34	
	6	48	90	320	1.88	6.67	0.26	0.31	
EPON 962	2	33	19	345	0.58	10.45	0.06	0.29	59
	4	33	37	435	1.11	13.18	0.08	0.28	
	6	33	58	574	1.74	17.39	0.10	0.29	

Compressive modulus and strength results were normalized to a V_f of 50% by dividing the experimentally measured result by the actual V_f (percent) and multiplying by 0.50. Actual V_f values, determined based on the known fiber areal volume wound onto the mandrel and the cured cylinder thickness, ranged from 47% to 59%, with the epoxy-based specimens at the top of the range due to relatively abundant matrix drip-off (Table). Five laminates were evaluated for each material system with 3 $[0_n/90_n]_s$ variations of undulation amplitude and 2 $[30_n/–60_n]_s$ variations of undulation amplitude.

Specimens were tested on an MTS Model 810 hydraulic test frame at a rate of 1.27 mm/min (0.05 inch/min). A 89-kN (20-kip) load cell was used to measure applied load. Two-dimensional DIC was used to measure the surface displacement/deformation of the specimen under load. DIC measures the displacement of contrasting features in a random speckle pattern painted on the surface of the specimen.[27,28] In-plane strains were calculated from the in-plane displacements using the program Vic 2D (Correlated Solutions Inc., Columbia, SC). The speckle pattern was created using commercially available flat black and white spray paints, which provide the largest color/brightness contrast in grayscale coloring. A step size of 15 and a subset of 30 were used during image correlation. A size 5 strain filter and Lagrange tensor type were used. The area of interest was nominally 25.4 mm wide × 25.4 mm tall. For the GRAS-50S5M (2,448 × 2,048 pixels), the spatial resolution was 96 × 81 pixels/mm.

Model 647.10A hydraulic wedge grips were used to compressively load specimens through combined shear traction and end loading. Glass/epoxy tabs were placed on the ends of the specimen to protect it from damage due to high gripping pressure. ASTM D 3410[29] was referenced in determining the minimum specimen gage length to avoid global buckling of the specimen. A florescent lamp was used to provide area illumination to the speckled surface of the specimen in the area of interest. Cameras were placed approximately 61 cm (24 inches) from the test specimen to common walkways (Fig. 8). Nikon 28- to 105-mm (1.1- to 4.1-inch) focal length lenses were used in focusing the image of the specimen.

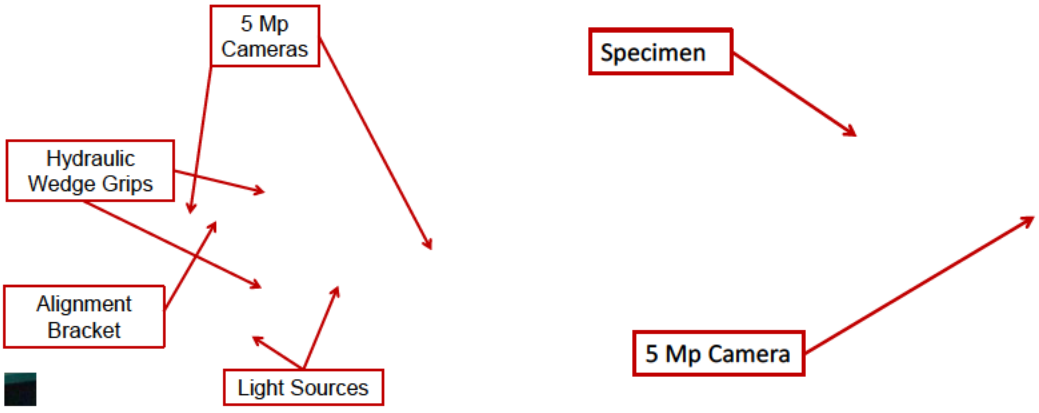

Fig. 8 Compression test setup

3. Results and Discussion

Figure 9 shows representative axial strain fields (ε_{xx}) for compressively loaded $[0_n/90_n]_s$ specimens with various undulation amplitudes. The loading direction is horizontal and the axial stress at which the images were obtained was roughly 50% of the ultimate strength. The dark dashed line represents the path of the undulating 0° ply. The location of the highest axial strain (i.e., largest negative strain, highlighted with a light dashed circle) appears where the 0° ply subducts under the 90° ply in the underlying 90° ply. The region of lowest axial strain (i.e., least negative strain, highlighted with a light dashed rectangle) appears in the 90° ply where the 0° plies meet at the mid-plane of the laminate. Such strain concentrations instigate the failure process of $[0_n/90_n]_s$ specimens. FMC specimens show this feature most readily because the unsupported length is about 2 times the undulation length. This places the undulated material sufficiently far away from the wedge grips. Due to the considerable compressive strength of RMCs, the unsupported length was reduced to a value that superposed grip-related strain disturbances with undulation-related strain disturbances.

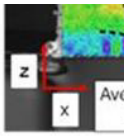

(a) LF750 (b) 30917 (c) EPON 862

Fig. 9 Axial normal strain, ε_{xx}, in $[0_n/90_n]_s$ specimens (loading in x-direction, length approximately 20 mm)

The same trends can be seen in the out-of-plane strain, ε_{zz}, where the higher magnitude strain (i.e., most positive strain, highlighted by light dashed circle) coincides with where the reinforcing 0° ply subducts under the 90° ply (Fig. 10). Lower-magnitude out-of-plane strains coalesce at the "end" of the undulation where the material returns to being laminated. Increased compressive loading leads to localization of high out-of-plane strains, ε_{zz}, near the 0° and 90° interface. Strain concentrations have been observed to occur at ply interfaces in composites without undulation.[30] The 30917 $[0_4/90_4]_s$ out-of-plane strain field in Fig. 10 features an early manifestation of this phenomenon. In general, specimens with larger undulation amplitude experience greater out-of-plane strains.

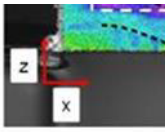

(a) LF750 (b) 30917 (c) EPON 862

Fig. 10 Out-of-plane normal strain, ε_{zz}, in $[0_n/90_n]_s$ specimens

Out-of-plane tensor shear strain, ε_{xz}, was antisymmetric about the midplane of the laminates, as may be expected, shown in Fig. 11 for $[0_6/90_6]_s$ (top) and $[30_4/–60_4]_s$ (bottom) specimens. Measurements were highest along the ply interfaces where mismatched ply properties can be expected to cause high strains. The shear strain was higher in the $[30_4/–60_4]_s$ laminate than in the $[0_6/90_6]_s$ laminate and was higher in softer matrixes than in stiffer matrixes.

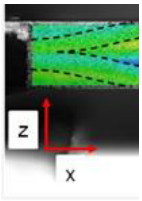

Fig. 11 Out-of-plane tensor shear strains, ε_{xz}, in $[0_6/90_6]_s$ and $[30_4/–60_4]_s$ specimens

DIC results for $[30_n/–60_n]_s$ laminates showed similar axial (Fig. 12) and out-of-plane normal (Fig. 13) strain field response as the $[0_n/90_n]_s$ tests. That is, the highest-magnitude strains were observed in the middle –60° plies where the 30° surface plies begin to subduct (light dashed circle). The lowest magnitude strains were seen in a broad area near where the 30° plies meet at the midplane (light dashed rectangle). As expected, greater undulation amplitude and matrix material compliance increase the strain amplitude in both the axial and out-of-plane directions. The out-of-plane normal strain field also shows high magnitude concentrations at the ply interfaces, as seen in the $[0_n/90_n]_s$ specimens.

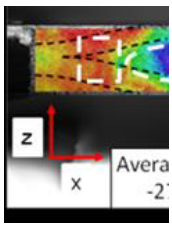

Fig. 12 Axial normal strains, ε_{xx}, in $[30_n/–60_n]_s$ specimens

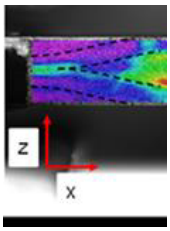

Fig. 13 Out-of-plane normal strains, ε_{zz}, in $[30_n/–60_n]_s$ specimens

Axial stress-strain curves were observed to be approximately linear for specimens without undulation (Fig. 14). Each point plotted in the stress-strain graphs represents the average value of strain across the undulated region of the specimen. The highest value of stress plotted for the nonundulated specimens corresponded with failure near the grip. For the undulated specimens, the highest value of axial stress plotted corresponded to fiber microbuckling away from the grips. Increasing the undulation amplitude ($n = 2 \rightarrow 6$) decreases both the strength and the modulus compared with the nonundulated case. Several differences between FMC and RMC response due to fiber undulation can be observed in Fig. 14. The strength difference between specimens with increasing undulation can be seen to be greater for FMC specimens than for the RMC specimens. Fiber undulation also causes moderate nonlinearity in the stress-strain curves in FMCs but not in RMCs.

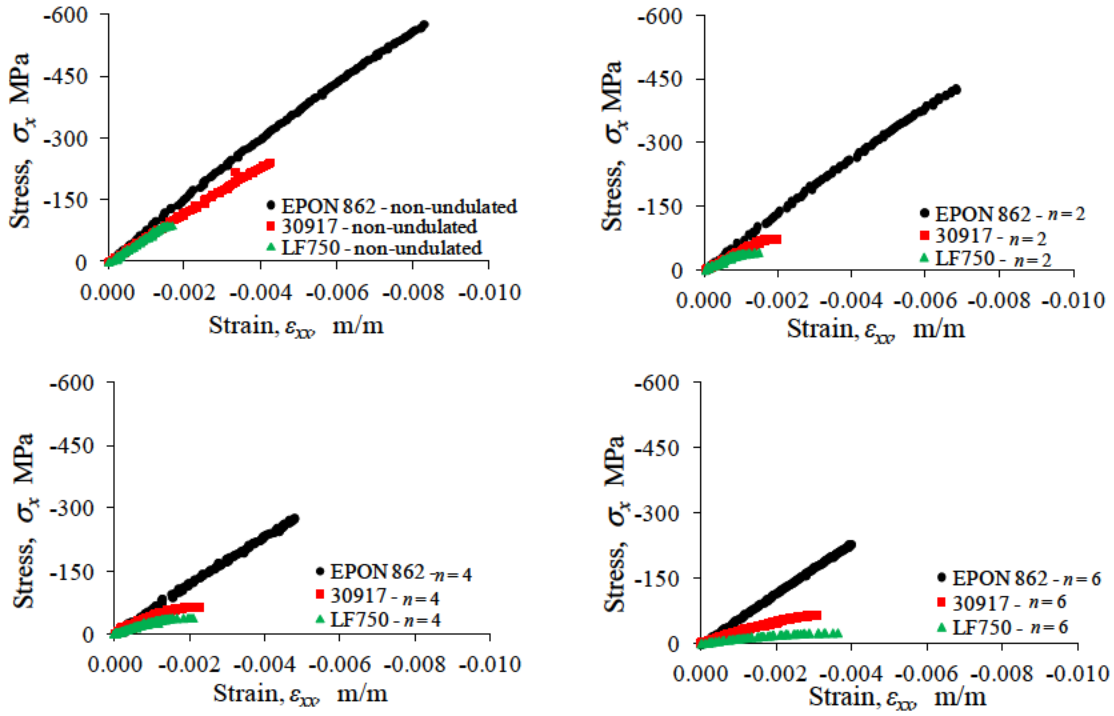

Fig. 14 Axial stress vs. axial strain: $[0_n/90_n]_s$

The axial modulus of unidirectional specimens is commonly considered a fiber-dominated property. So, as expected, specimens with no fiber undulation (undulation amplitude/length = 0) had approximately the same modulus regardless of the matrix material (Fig. 15). In the presence of undulation, specimens with a stiffer matrix material retained a larger percentage of the nonundulated modulus. This result suggests that fiber undulation causes E_x to be more highly influenced by the matrix possibly through the contributions of the out-of-plane shear modulus of the composite and the out-of-plane fiber orientation from the undulation.[11,13]

For the range of undulation amplitude/length ratios investigated, both polyurethane matrixes showed little change in compressive strength. It is hypothesized that changes in strength come from a change in the failure mode caused by the introduction of undulation.[13] In the nonundulated case, the failure mode is likely to be fiber microbuckling or kinking. As undulation is introduced in increasing amplitudes, the failure mode is increasingly influenced by out-of-plane shear, which reduces the axial strength of the composite. The undulation amplitude/length ratios obtained in the FMCs appear to be too large to observe the transition in failure mode.

The $[30_n/–60_n]_s$ axial stiffness and strength are largely independent of the undulation geometry (Fig. 15). This result suggests that the off-axis orientation of the fibers in the plane of the laminate (30°–60°) is more detrimental to the axial properties than out-of-plane orientation of the fibers (5°–20°) in the undulated region. For the same undulation size and fiber volume fraction, stiffer matrix systems are stiffer and stronger than their more compliant counterparts.

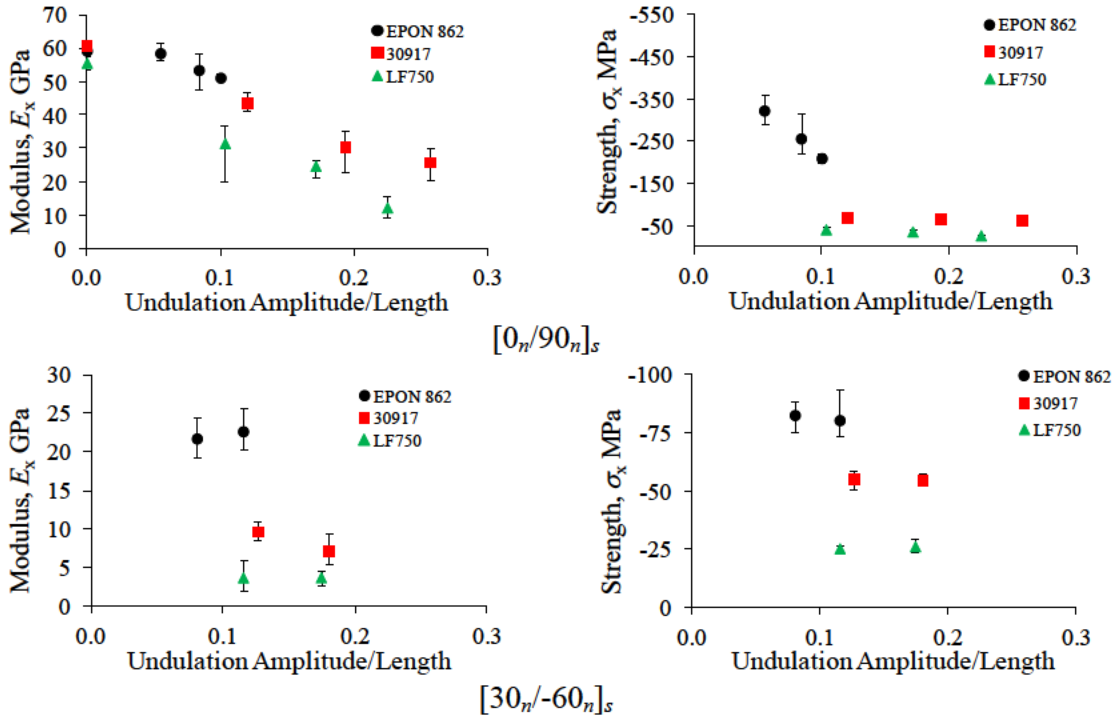

Fig. 15 Modulus and strength vs. wave amplitude/wave length

DIC data also facilitated understanding of the failure mode associated with undulated fibers. A typical stress strain curve for an LF750 $[0_6/90_6]_s$ specimen along with DIC images at 3 stages of loading (A, B, C) are shown in Fig. 16. At the approximate onset of nonlinearity (Stage A), the strain fields resemble those shown previously.

State B represents a significant change in the stress-strain behavior of the specimen. Damage onset is indicated by large out-of-plane normal strain, ε_{zz}, which signifies delamination in the regions highlighted by a light dashed circle. This damaged area increases the axial strain, ε_{xx}, in the undulating fiber. With the out-of-plane stiffness now reduced due to delamination, the misalignment of the fiber increases until microbuckling occurs. Microbuckling can be observed at Stage C, where the undulating fibers have displaced in the positive z-direction within the light dashed circle. Strain components ε_{xx}, ε_{zz}, and ε_{xz} are approximately 4, 10, and 8 times higher, respectively, near the microbuckled area at Stage C versus the same area at Stage A.

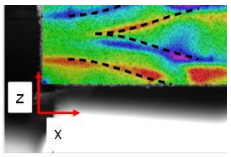

(A) (B) (C)

Fig. 16 Strain stages at A, B, and C in an LF750 $[0_6/90_6]_s$ specimen

4. Conclusions

Ply undulation was detrimental to the axial compressive modulus and strength of FMC and RMC $[0_n/90_n]_s$ specimens. FMCs were more sensitive to fiber undulation than RMCs. An undulation with an amplitude/length ratio of 0.1 reduces the longitudinal modulus of elasticity in the undulation region by approximately 43%, 28%, and 3% in specimens with LF750, 30917, and EPON 862 resins, respectively, relative to specimens without undulation. Specimens without undulations were observed to have approximately the same modulus regardless of the matrix material. For the range of undulation amplitude/length investigated, both polyurethane resins showed little change in axial strength.

The $[30_n/–60_n]_s$ specimens were more strongly dominated by the composite shear properties, which were very different depending on matrix material. Modulus and strength of the $[30_n/–60_n]_s$ specimens were largely independent of undulation amplitude. This result suggests that the introduction of fiber undulation most critically affects fiber-dominated properties (modulus and strength of $[0_n/90_n]_s$ specimens). For the same undulation size and fiber volume fraction, stiffer matrix systems are stiffer and stronger than their more compliant counterparts.

For both laminates, strain concentrations were of highest magnitude at the location where the undulating ply subducts beneath the surface of the laminate. Conversely, strain concentrations were low where the undulating plies met in the middle of the laminate. It was observed that the

introduction of undulation itself does not greatly increase the axial strain in the reinforcing fibers prior to microbuckling where the fiber subducts from the surface to the interior. Rather, the other strain components (out-of-plane shear and out-of-plane normal strains) increase considerably where the subduction begins, eventually leading to delamination. Delamination decreases out-of-plane stiffness, increasing the misalignment of the fiber until microbuckling occurs.

5. References

1. Mayrides B, Wang KW, Smith EC. Analysis and synthesis of highly flexible helicopter drivelines with flexible matrix composite shafting. Proceedings of the 61st American Helicopter Society Annual Forum; 2005 Jun 1–3; Grapevine, TX. Alexandria (VA): American Helicopter Society. p. 1582–1595.
2. Hannibal AJ, Gupta BP, Avila JA, Parr CH. Flexible matrix composites applied to bearingless rotor system. Journal of the American Helicopter Society. 1985;30(1):21–27.
3. Ocalan M. High flexibility rotorcraft driveshafts using flexible matrix composites and active bearing control [thesis]. [University Park (PA)]: The Pennsylvania State University; 2002.
4. Shin E, Wang KW, Smith EC. Characterization of flexible matrix composite rotorcraft driveshafts. Proceedings of the 59st American Helicopter Society Annual Forum; 2003 Jun 1–3; Grapevine, TX. Alexandria (VA): American Helicopter Society. p. 1961–1968.
5. Roos C, Bakis CE. Multi-physics design and optimization of flexible matrix composite driveshafts. Composite Structures. 2011;93:2231–2240.
6. Henry TC, Bakis CE, Smith EC. Determination of effective ply-level properties of filament wound composite tubes loaded in compression. Journal of Testing and Evaluation. 2015;43(1):1–12.
7. Ishikawa T, Chou T. Stiffness and strength behavior of woven fabric composites. Journal of Materials Science. 1982;12:3211–3220.
8. Morozov EV. The effect of filament-winding mosaic patterns on the strength of thin-walled composite shells. Composite Structures. 2006;76:123–129.
9. Zhang Y, Xia Z, Ellyin F. Two-scale analysis of a filament-wound cylindrical structure and application of periodic boundary conditions. International Journal of Solids and Structures. 2008;45:5322–5336.
10. Hipp P, Jensen D. Design and analysis of filament-wound cylinders in compression. Proceedings of the 33rd AIAA/ASME/ASCE/AHS/ASC Structures, Structural Dynamics, and Material Conference; 1992; Dallas, TX. Reston (VA): American Institute of Aeronautics and Astronautics. p. 2442–2452. Paper No.: AIAA-92-2307.
11. Jensen D, Pai S. Influence of local fiber undulation on the global buckling of filament-wound cylinders. Journal of Reinforced Plastics and Composites. 1993;12:865–875.

12. Pai SP, Jensen DW. Influence of fiber undulations on buckling of thin filament-wound cylinders in axial compression. Journal of Aerospace Engineering. 2001;14(1):12–20.

13. Bogetti TA, Gillespie JW, Lamontia MA. Influence of ply waviness on the stiffness and strength reduction on composite laminates. Journal of Thermoplastic Composite Materials. 1992;5:344–369.

14. Rosen BW, Mechanics of composite strengthening. In: Bush SH, editor. Fiber composite materials. Novelty (OH): American Society for Metals; 1965. p. 37–75.

15. Yurgartis SW. Measurement of small angle fiber misalignments in continuous fiber composites. Composite Science and Technology. 1987;30:279–293.

16. Lo KH, Chim ESM. Compressive strength of unidirectional composites. Journal of Reinforced Plastics and Composites. 1992;11(8);838–896.

17. Adams DO, Bell SJ. Compression strength reductions in composite laminates due to multiple-layer waviness. Composites Science and Technology. 1995;53:207–212.

18. Xu YL, Reifsnider KL. Micromechnical modeling of composite compressive strength. Journal of Composite Materials. 1993;27:572–588.

19. Naik NK, Kumar RS. Compressive strength of unidirectional composites: evaluation and comparison of prediction models. Composite Structures. 1999;46:299–308.

20. Scheuer R, Mertiny P, Bormann D. Analysis of surface strains and leakage behavior in composite pipes and vessels using digital image correlation technique. PVP 2009. Proceedings of the Pressure Vessels and Piping Conference; 2009 Jul 26–30; Prague, Czech Republic. New York (NY): American Society of Mechanical Engineers. Vol. 5; p. 449–455. Paper No.: PVP2009-77522.

21. Crouzeix L, Torres M, Douchin B, Périé JN, Collombet F, Hernández H. 2009. Assessment of the winding pattern effects on the behaviour of filament wound pipes by using full field measurements and the equilibrium gap method. ICCM-17. Proceedings of the 17th International Conference on Composite Materials; 2009 Jul 27–31; Edinburgh, Scotland. London (England): The Institute of Materials, Minerals and Mining.

22. Henry TC, Bakis CE, Emerson RP, Riddick JC. Characterization of compressively loaded filament wound composite cylinders using digital image correlation. Reinforced Plastics and Composites Institute Proceedings of the 28th Technical Conference, American Society of Composites; 2013. Lancaster (PA): DEStech Publications; c2013. CD ROM.

23. Sollenberger SG, Bail JL, Kohlman L, Ruggeri CR, Bakis CE, Roberts GD, Smith EC. Ballistic impact tolerance of filament-wound composite tubes with rigid and flexible matrix material. In: Lanz JB, Takeda N, Doudican BM, Schoeppner GA, Donaldson, SL, editors. Proceedings of the 25th Technical Conference. American Society for Composites; 2010 Sep 22–23; Dayton, OH. Lancaster (PA): DEStech Publications; c2010. CD ROM.

24. Torres M, Crouzeix L, Douchin B, Collombet F, Hernández H, González J. Strain field measurement of filament-wound composites at ±55° using digital image correlation: an approach for unit cells employing flat specimens. Composite Structures. 2010;92:2457–2464.

25. Makeev A, Seon G, Lee E. Failure predictions for carbon/epoxy tape laminates with wavy plies. Journal of Composite Materials. 2009;44:95–112.

26. Henry TC. Static and dynamic characterization of composite materials for future driveshaft design [thesis]. [University Park (PA)]: The Pennsylvania State University; 2012.

27. Chu TC, Ranson WF, Sutton MA, Peters WH. Applications of digital-image-correlation techniques to experimental mechanics. Experimental Mechanics. 1995;25(3):232–244.

28. Sutton MA, Wolters WJ, Peters WH, Ranson WF, McNeill WR. Determination of displacements using an improved digital image correlation method. Computer Vision. 1983;1(3):133–139.

29. ASTM Standard D 3410. Standard test method for compressive properties of polymer matrix composite materials with unsupported gage section by shear loading. West Conshohocken (PA): ASTM International; 2010.

30. Herakovich CT, Post D, Buczek MB, Czarnek R. Free edge strain concentrations in real composite laminates: experimental-theoretical correlation. Journal of Applied Mechanics. 1985;52:787–793.

1 (PDF) DEFENSE TECHNICAL INFORMATION CTR DTIC OCA

2 (PDF) DIRECTOR US ARMY RESEARCH LAB RDRL CIO LL IMAL HRA MAIL & RECORDS MGMT

1 (PDF) GOVT PRINTG OFC A MALHOTRA

1 HC PROFESSOR CHARLES E. BAKIS DEPT. OF ENGINEERING SCIENCE & MECHANICS PENN STATE UNIV 212 EES BLDG UNIV PARK PA 16802

3 HC DIR USARL RDRL VTM T HENRY J C RIDDICK D LE 4603 FLARE LOOP APG MD 21005

1 HC DIR USARL RDRL WMM A R EMERSON